Int. J. Appl. Math. Comput. Sci., 2024, Vol. 34, No. 1, 105–117
DOI: 10.61822/amcs-2024-0008

REMAINING USEFUL LIFE PREDICTION OF A LITHIUM–ION BATTERY BASED ON A TEMPORAL CONVOLUTIONAL NETWORK WITH DATA EXTENSION

JING ZHAO [a,b], DAYONG LIU [a,c,*], LINGSHUAI MENG [a,c]

[a] Shenyang Institute of Automation
Chinese Academy of Sciences
Shenyang 110016, China
e-mail: liudayong@sia.cn

[b] Institute of Robotics and Intelligent Manufacturing
Chinese Academy of Sciences
Shenyang 110169, China
e-mail: zhaojing@sia.cn

[c] University of the Chinese Academy of Sciences
Beijing 100049, China

Unmanned underwater vehicles are typically deployed in deep sea environments, which present unique working conditions. Lithium-ion power batteries are crucial for powering underwater vehicles, and it is vital to accurately predict their remaining useful life (RUL) to maintain system reliability and safety. We propose a residual life prediction model framework based on complete ensemble empirical mode decomposition with an adaptive noise-temporal convolutional net (CEEMDAN-TCN), which utilizes dilated causal convolutions to improve the model's ability to capture local capacity regeneration and enhance the overall prediction accuracy. CEEMDAN is employed to denoise the data and prevent RUL prediction errors caused by local regeneration, and feature expansion is utilized to extend the temporal dimension of the original data. The NASA and CALCE battery capacity datasets are used as input to train the network framework. The output is the current predicted residual capacity, which is compared with the real residual battery capacity. The MAE, RMSE and RE are used as the evaluation indexes of the RUL prediction performance. The proposed network model is verified on the NASA and CACLE datasets. The evaluation results show that our method has better life prediction performance. At the same time, it is proved that both feature expansion and modal decomposition can improve the generalization ability of the model, which is very useful in industrial scenarios.

Keywords: lithium-ion battery, remaining useful life, complete EEMD with adaptive noise, temporal convolutional net.

1. Introduction

Unmanned underwater vehicles (UUVs) are increasingly being utilized in marine engineering projects as a pivotal instrument for human cognition and ocean exploration, particularly in deep sea environments. Effective operation of UUVs necessitates a power source with the requisite levels of stability and endurance.

Lithium-ion batteries have emerged as the predominant power source for underwater robots, owing to their exceptional features such as high power, capacity, and energy density, as well as their ability to avoid memory effects, exhibit low self-discharge rates, and sustain long recyclable lifetimes. The performance of lithium-ion batteries will be decreased as the battery is continually cycled due to obstruction of its internal diaphragm, which results in a steady loss in its capacity and increases the risk of failure or fire (Hong *et al.*, 2022).

As a result, it has become critically important to predict the remaining useful life (RUL) of Li-ion batteries with precision, to ensure secure and stable operation of

*Corresponding author

energy storage systems. A thorough understanding of the factors that influence the RUL of such batteries can significantly enhance the reliability and safety of UUVs and other underwater robotic systems.

Currently, there are two main methods for predicting the remaining useful life of lithium-ion batteries: model-driven and data-driven approaches (Cao *et al*., 2021). The former predict battery RUL by constructing a model of the battery capacity decline. This method is well-established and has reached a relatively mature stage of development (Seybold *et al*., 2015). In contrast, the latter approaches do not require a complex battery model, but instead investigate the relationship between external parameters and internal states to infer the battery RUL.

Owing to its robust feature extraction and nonlinear trend approximation capabilities, a family of neural networks have been widely employed in the domain of the RUL prediction. As RUL primarily entails a regression problem involving time series data, the innate capacity of a model to effectively learn temporal information is vital to its predictive performance (Ye and Dai, 2018). Recently, recurrent neural networks (RNNs) and their various derivatives (e.g., LSTM, GRU, etc.) have gained prominence in the field of prognostics and health management (PHM) due to their ability to fully leverage temporal information.

To develop a lifetime prediction model for lithium-ion batteries, Park *et al*. (2020) integrated the long short-term memory (LSTM) technique with multiple measured data types, including voltage, current, temperature, and charging curve. Li *et al*. (2019) employed a long short-term memory recurrent neural network (LSTM-RNN) to uncover the long-term dependence of lithium-ion battery capacity degradation. Addressing the issue of capacity regeneration during the lithium battery life decline, Zhang *et al*. (2018) combined empirical mode decomposition (EMD) with LSTM and Elman neural networks. They utilized the EMD method to decompose battery capacity sequences into intrinsic mode functions (IMFs), and constructed low-frequency and high-frequency prediction models for capacity data. To tackle the time series prediction challenge, Bai *et al*. (2018) introduced a temporal convolutional network (TCN) algorithm, demonstrating its superior performance over traditional recursive architectures such as LSTM and RNNs. In an effort to mitigate the RUL prediction errors caused by local regeneration, Zhou and Huang (2016) proposed a prediction model based on the TCN and employed the EMD technique for data denoising, resulting in a model with minimal starting point dependence, high prediction accuracy, and robustness.

The conventional EMD algorithm is prone to modal confusion during the smoothing process, hindering accurate battery lifetime predictions based on capacity degradation rates. In contrast, the complete ensemble EMD with adaptive noise (CEEMDAN) algorithm incorporates white noise's IMF components into each decomposition. To extract complex sequence fluctuation patterns, the added noise's IMF component is gradually diminished, simultaneously reducing residual noise in the intrinsic modal components. This effectively lowers the reconstruction error, enhances decomposition, and yields improved prediction outcomes. Upon extensive testing and analysis, the TCN model outperforms the LSTM and GRU baseline models in terms of prediction accuracy and resilience, demonstrating its potential to capture local regeneration phenomena in RUL prediction.

The main contribution of the study can be attributed to the following three aspects:

1. Based on the TCN network, this paper proposes a convolutional network structure for time series to improve the accuracy of time series.

2. At present, the combination of RNNs or multiple traditional models is commonly used to reduce the rebound effect of battery capacity. This paper proposes a new improvement idea, which can more effectively solve the influence of this phenomenon on battery RUL prediction and improve the robustness of the model.

3. Combined with CEEMDAN, the global degradation and local regeneration of battery capacity are separated, and this process mitigates the influence of the original data's volatile components and extends the training set sample features by increasing the sample count in the feature dimension based on the original time series dimension, which improves the prediction accuracy of the TCN model of lithium-ion battery RUL.

2. Capacity degradation dataset

2.1. RUL prediction results and analysis.

2.1.1. RUL definition. The remaining useful life predictor is an essential tool for battery risk notification (Zhou *et al*., 2020). The state of health (SOH) of a battery is a health indicator of battery ageing, representing the battery's condition during each charge-discharge cycle (Park *et al*., 2020). RUL is defined as the capacity ratio

$$SOH = \frac{C_t}{C_0} \times 100\%, \tag{1}$$

where C_0 denotes the rated capacity and C_t stands for the measured capacity of cycle t.

The capacity of a battery decreases with increased charging and discharging. The end of life (EOL), which is closely related to a battery's capacity (Chen *et al*., 2022),

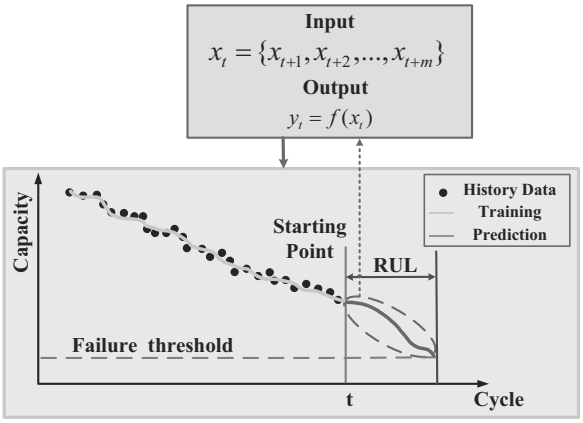

Fig. 1. Example of RUL prediction.

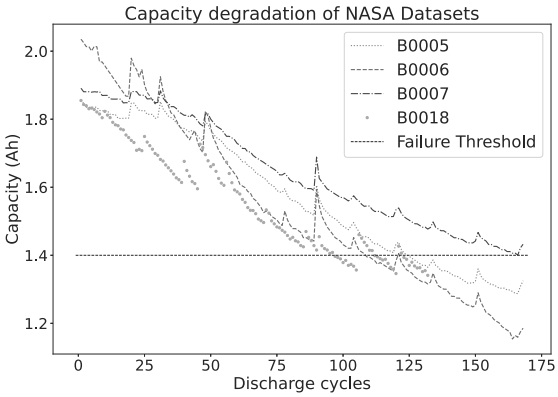

Fig. 2. NASA dataset battery capacity degradation curve.

is characterized as the time when the battery's remaining capacity reaches 70–80% of its initial capacity. Figure 1 illustrates an RUL prediction.

2.2. Dataset.

2.2.1. NASA dataset. The National Aeronautics and Space Administration (NASA) provided an open dataset of lithium-ion batteries for this study, and four groups of batteries labeled B0005, B0006, B0007, and B0018 were selected as the research objects (Saha and Goebel, 2007).

The charging process was conducted at a constant voltage of 4.2 V until the battery voltage reached 1.5 V, at which point the charging current was reduced to 20 mA (Ren *et al*., 2018). The batteries were tested at a temperature of 24°C. Batteries B0005, B0006, B0007 and B0018 were discharged using a continuous current mode of 2 A until their voltages fell to 2.7 V, 2.5 V, 2.2 V and 2.5 V, respectively. A battery was considered to have reached the end of its useful life when its rated capacity fell to 30% of its initial capacity or when it reached a capacity between 2 Ah and 1.4 Ah.

Figure 2 illustrates the variation in battery capacity for the four groups of batteries with respect to the number of charging and discharging cycles. Detailed information on the NASA batteries is presented in Table 1.

2.2.2. CALCE dataset. For this study, four batteries were selected from the battery cycle test dataset (CALCE) of the Advanced Life Cycle Engineering Center at the University of Maryland, namely, CS2_35, CS2_36, CS2_37 and CS2_38 (Pecht, 2017).

The battery voltage was charged in a constant current mode of 1 C until it reached 4.2 V, while the testing temperature was 1°C. Once the charging current reached 50 mA, the battery was charged in constant voltage mode. The battery voltage was discharged in continuous current mode at 1 C until it reached 2.7 V. A battery was considered to have reached the end of its useful life when its rated capacity reduced to 30% of its initial capacity, ranging from 1.1 Ah to 0.77 Ah.

Figure 3 depicts the battery capacity degradation curve for the four selected batteries as they approached the end of their useful life. Detailed information on the CALCE batteries is presented in Table 2.

3. Basic theories and methods

3.1. CEEMDAN. Huang *et al*. (1998) proposed an adaptive signal time-frequency processing method known as empirical mode decomposition (EMD), which decomposes signals based on their intrinsic time scale without the need for any pre-set basis functions (Cao *et al*., 2019).

Despite the advantages of EMD in handling nonstationary and nonlinear signals, it still suffers from the problem of "mode mixing." Mode mixing refers to the presence of oscillations with similar amplitudes across modes, or vice versa. The ensemble empirical mode decomposition (EEMD) algorithm effectively reduces mode mixing in the EMD algorithm by incorporating Gaussian white noise into the data (Wu and Huang, 2009). However, after signal reconstruction, the EEMD method cannot completely eliminate Gaussian white noise, resulting in reconstruction errors.

Building on EMD and EEMD methods, the CEEMDAN theory was developed, which successfully addresses the issues of mode aliasing, incomplete decomposition, and significant reconstruction errors. It offers the benefits of fast operation speed, a good mode spectrum separation effect, and small reconstruction errors (Torres *et al*., 2011; Huang *et al*., 1998) and is frequently used for non-stationary and nonlinear data processing. The specific steps of CEEMDAN are as follows:

Table 1. Parameters for the NASA lithium-ion batteries.

Battery	Test temperature	Minimal charge current	Constant discharge current	Initial/cut-off rated capacity	Charge/discharge cut-off voltage
B0005	24 °C	20 mA	2 A	2 Ah/1.4 Ah	4.2 V/2.7 V
B0006	24 °C	20 mA	2 A	2 Ah/1.4 Ah	4.2 V/2.5 V
B0007	24 °C	20 mA	2 A	2 Ah/1.4 Ah	4.2 V/2.2 V
B0018	24 °C	20 mA	2 A	2 Ah/1.4 Ah	4.2 V/2.5 V

Table 2. Parameters for the CALCE lithium-ion batteries.

Battery	Test temperature	Minimal charge current	Constant discharge current	Initial/cut-off rated capacity	Charge/discharge cut-off voltage
CS2_35	1°C	50 mA	1 C	1.1 Ah/0.77 Ah	4.2 V/2.7 V
CS2_36	1°C	50 mA	1 C	1.1 Ah/0.77 Ah	4.2 V/2.7 V
CS2_37	1°C	50 mA	1 C	1.1 Ah/0.77 Ah	4.2 V/2.7 V
CS2_38	1°C	50 mA	1 C	1.1 Ah/0.77 Ah	4.2 V/2.7 V

Step 1. Adding white Gaussian noise $\varepsilon_0\omega_i(t)$ with the initial amplitude of ε_0 to the Lithium-ion battery capacity sequence $S(t)$, $S_i(t) = S(t) + \varepsilon_0\omega_i(t)$, $(i = 1, 2, \ldots, I)$ can be obtained; using EMD to decompose $S_i(t)$ to get i modal components IMF_1^i in the first stage, and take the average value of IMF_1 to get the first modal component $\overline{\mathrm{IMF}}_1$ as

$$\overline{\mathrm{IMF}}_1 = \frac{1}{I}\sum_{i=1}^{I}\mathrm{IMF}_1^i. \tag{2}$$

Step 2. Calculate the first residual as

$$R_1(t) = S_i(t) - \overline{\mathrm{IMF}}_1. \tag{3}$$

Step 3. Use $E_k(\cdot)$ to represent the k-th modal component obtained after EMD processing, and decompose the signal $R_1(t) + \varepsilon_1 E_1(\omega_i(t))$ to obtain the second modal component as

$$\overline{\mathrm{IMF}}_2 = \frac{1}{I}\sum_{i=1}^{I} E_1\left(R_1(t) + \varepsilon_1 E_1(\omega_i(t))\right). \tag{4}$$

Step 4. For $k = 1, 2, \ldots, n$, calculate the k-th residual as

$$R_k(t) = R_{k-1}(t) - \overline{\mathrm{IMF}}_k. \tag{5}$$

Step 5. The signal $R_k(t) + \varepsilon_k E_k(\omega_i(t))$ is decomposed and the $(k+10)$-th modal component is

$$\overline{\mathrm{IMF}_{k+1}} = \frac{1}{I}\sum_{i=1}^{I} E_1\left(R_k(t) + \varepsilon_k E_k(\omega_i(t))\right). \tag{6}$$

Step 6. Steps 4 and 5 is repeated until the final $R_n(t)$ cannot be decomposed, and the final residual is obtained as

$$R_n(t) = S_i(t) - \sum_{k=1}^{n}\overline{\mathrm{IMF}}_k, \tag{7}$$

where n is the total number of modal components.

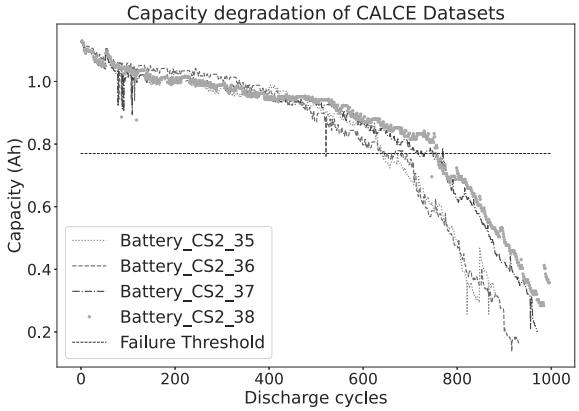

Fig. 3. CALCE dataset battery capacity degradation curve.

3.2. Temporal convolutional network (TCN). The temporal convolutional network (Bai *et al.*, 2018), which is a descendant of the convolutional neural network (CNN), is made up of 1D convolutional layers with inflated causality and the identical input and output lengths. It is well suited for processing time series data. In order to fulfill the two conditions for processing timing issues the following is performed:

(a) The network begins predicting with the input $x_0, \ldots, x_t$, and outputs $y_0, \ldots, y_t$ of the same size; x represents the data on lithium battery capacity, and y represents the projected lithium battery capacity.

(b) Temporal prediction necessitates that the forecast of y_t at time t can only be assessed by the input of x_1 to x_{t-1} before time t.

The temporal convolutional network (TCN) is primarily composed of three core components (Li *et al.*,

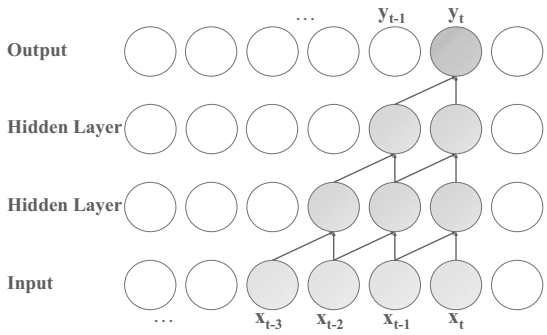

Fig. 4. Causal convolution.

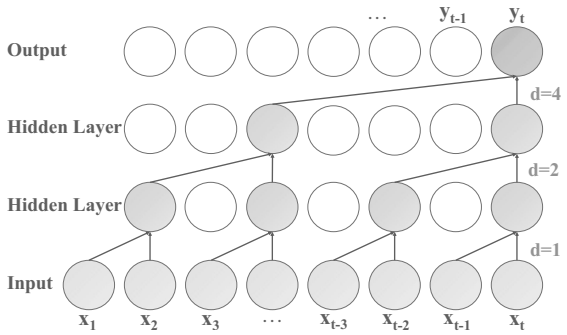

Fig. 5. Dilated convolution.

2023): causal convolution dilated convolution, and a residual block.

Causal convolution. To overcome the issue of potential data leakage in battery capacity predictions, the TCN incorporates causal convolutions as shown in Fig. 4. This approach ensures that only past data prior to the prediction time t are utilized in generating predictions, as captured by the following formula for causal convolution:

$$P\left(x_t\right) = \prod_{t=1}^{T} P\left(x_t \mid x_1, x_2, \ldots, x_{t-1}\right). \tag{8}$$

Here $P(x_t)$ denotes the estimated probability while T represents the total duration or number of moments under consideration.

Dilated convolution. Using only causal convolution for historical capacity data in the TCN leads to an increase in the network depth. To address this issue, the TCN employs dilation convolution, which enables the model to capture dependencies across longer input sequences.

The TCN convolution operation is based on one-dimensional convolution, with dilation allowing convolution of input interval sampling. The sampling rate is controlled by parameter d, as shown in Fig. 5.

As the dilation level d increases, the range of expansion grows, resulting in an exponential increase in the effective window size as layers are added. By using fewer convolution layers, the network can achieve a large receptive field

$$d = 2^i, \tag{9}$$

where i is the number of layers of the network.

Dilated convolution is calculated as

$$F\left(x_t\right) = \sum_{i=0}^{k-1} f(i) x_{t-d_i}, \tag{10}$$

where $F(x_t)$ represents the network output resulting from the dilated convolution process, while k signifies the filter's dimensions. Furthermore, $f(i)$ denotes the filtering operation being conducted, and $t - d_i$ implies that the convolution operation is solely applicable to previous input data.

Residual block. In the TCN, residual connections are employed in place of convolutional layers, enabling the transfer of experimental data across layers. Figure 6 illustrates a residual block (He *et al.*, 2016), which consists of two layers built of a convolution and a nonlinear mapping, with additional regularization networks, such as WeightNorm (Salimans and Kingma, 2016) and Dropout (Srivastava *et al.*, 2014), connected to each layer to enhance the generalization capability of the TCN structure.

The use of residual blocks can prevent the degradation of performance and gradient disappearance resulting from an increase in the network depth. By facilitating the flow of information through the network, residual connections improve the TCN ability to learn from long input sequences

It is obvious that the simple TCN layer connection has been replaced by the residual structure,

$$O = Activation(x + F(x)). \tag{11}$$

As the number of channels between x and $F(x)$ might not be the same, a 1×1 Conv1 was developed to perform a simple transformation on x so that the modified version of x and $F(x)$ can be added (Bai *et al.*, 2018).

The TCN offer several advantages, including the following:

(i) *Parallel processing.* The TCN can process data in parallel rather than sequentially, resulting in faster computations.

(ii) *Flexible receptive field.* The receptive field of a temporal convolutional network is dictated by factors such as the quantity of layers, the dimensions of the convolution kernel, and the dilation coefficient. These parameters can be tailored to suit specific requirements and limitations in diverse contexts.

(iii) *Stable gradients.* Unlike the recurrent neural network (RNN), the TCNs suffer less from the issue of gradient

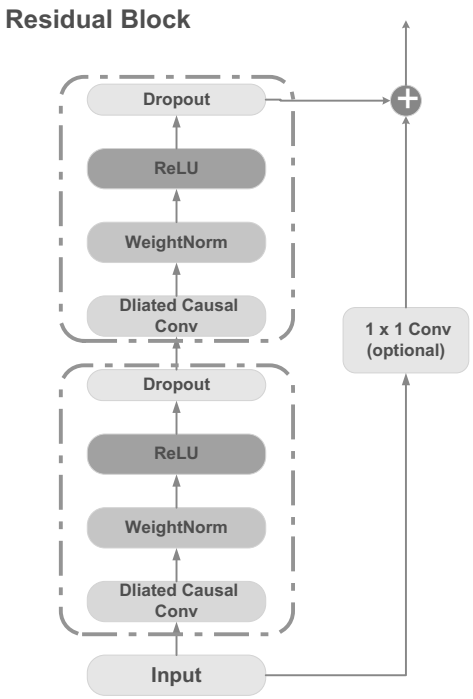

Fig. 6. Residual block of the TCN.

vanishing or exploding, making them more reliable in training and optimization.

(iv) *Memory efficiency.* When RNNs are employed, information from each time step must be stored, leading to high memory consumption. However, in the TCNs, the convolution kernel is shared across one layer, resulting in lower memory usage.

4. RUL prediction results and analysis

4.1. Analysis of the capacity sequence decomposition results of the CEEMDAN lithium-ion batteries. In this study, the capacity signal of lithium-ion batteries was decomposed into multiple intrinsic mode function (IMF) signals and a residual signal (Res), with frequencies arranged in descending order. Specifically, we utilized four groups of battery capacity attenuation data from the NASA and CALCE datasets. Figures 8 and 9 display the decomposition results of the battery capacity data and the resulting instantaneous frequencies of all IMFs, using batteries B0006 and CS2_35 as examples.

Figure 10 illustrates the results of using the CEEMDAN method for modal decomposition and data dimension expansion. It can be seen that the number of feature samples expands to four times the number of original data samples. By giving more diversity and flexibility to the model through data expansion, model generalization is improved, more data are used to train the

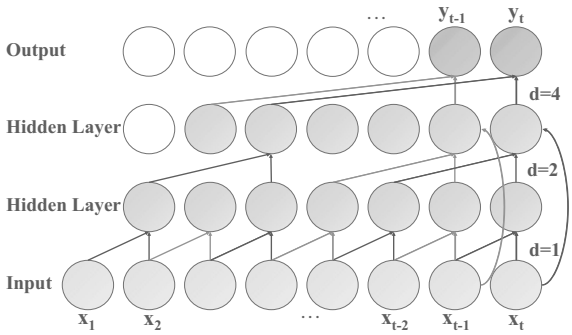

Fig. 7. Temporal convolutional network.

model, and the accuracy of the model in the prediction is improved.

The results show that the CS2_35 battery capacity mode decomposes into seven IMF components and one residual signal, while the B0006 battery capacity mode only decomposes into four IMF components and one residual signal. The components are arranged in descending order of instantaneous frequency, with the residual signal after decomposition removing interference from the capacity rebound phenomenon. This significantly reduces the negative effects of residual noise generation during the decline in the lithium-ion battery capacity, improving the reliability of battery life prediction.

However, signal decomposition may lead to some loss of original data, and using only the decomposed signals for training may result in inaccurate prediction results due to the inclusion of both real data information and noise. To address this issue, CEEMDAN mode decomposition was performed on the original data training and testing sets based on reconstructed signals, extending the sample characteristics of the training set to increase the feature dimension sample size while maintaining the original time series dimension. This approach helped us to enhance the prediction fitting precision of the neural network model.

4.2. Model prediction process design. CEEMDAN was employed to decompose the electric capacity data of all four battery groups into N components, denoted as IMF_i. The first two high-frequency components were then averaged and combined with the last trend component for data reconstruction.

One set of the reconstructed data was selected for analysis, while the remaining data were used as the training and validation sets. CEEMDAN was applied simultaneously to the training and validation sets, and the reconstructed data were added as a feature dimension to expand the dataset.

The expanded training and validation sets were used to fit the TCN network, and the neural network model was

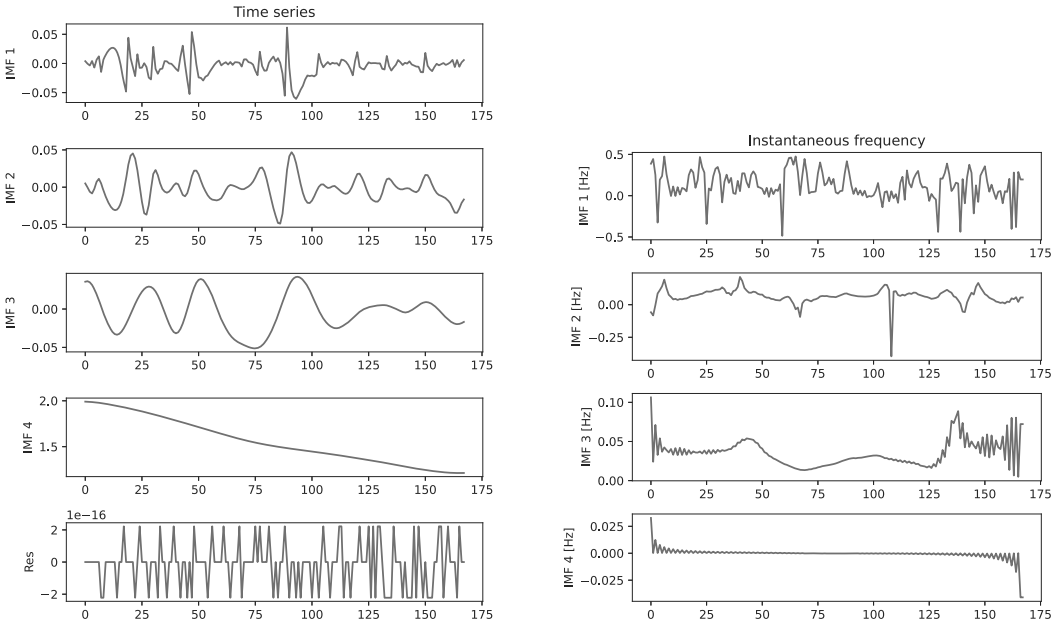

(a) (b)

Fig. 8. Modal components of B0006 battery capacity decomposition (a) and instantaneous frequency (b).

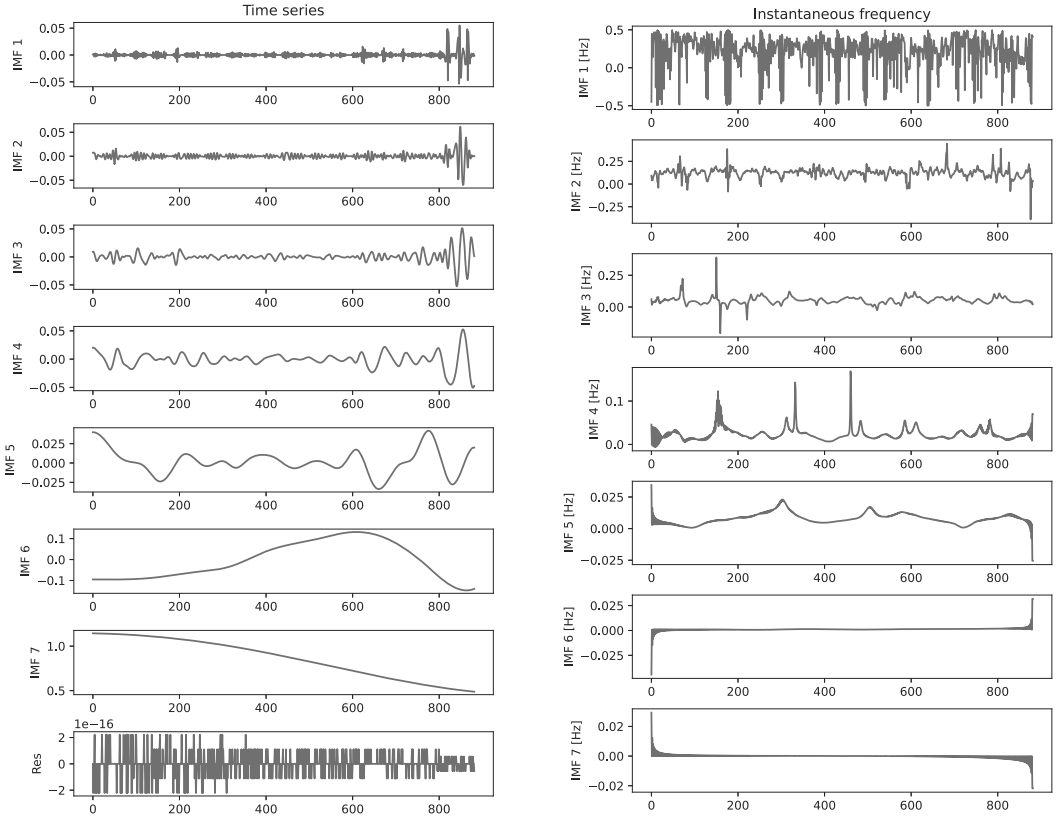

(a) (b)

Fig. 9. Modal components of CS2_35 battery capacity decomposition (a) and instantaneous frequency (b).

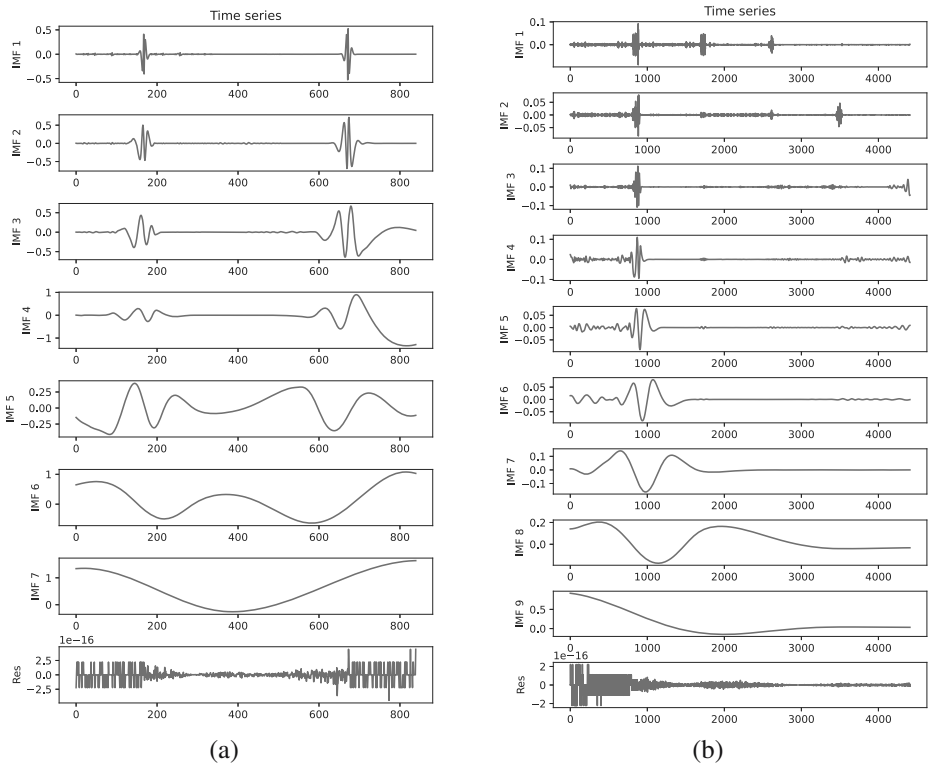

(a) (b)

Fig. 10. Datasets extension rendering based on the CEEMDAN method: NASA datasets (a), CALCE datasets (b).

established and utilized for prediction. The performance of the prediction model was evaluated using actual data, which served as the evaluation criterion.

4.3. Model evaluation. In order to comprehensively analyze the effectiveness of the selected method, the mean absolute error (MAE), relative error (RE) and root mean square error (RMSE) are selected as model evaluation indexes in this paper, and the calculation formula are as follows:

$$\mathrm{MAE} = \frac{1}{n}\sum_{t=1}^{n} |C_t - \widehat{C}_t|, \tag{12}$$

$$\mathrm{RMSE} = \sqrt{\frac{1}{n}\sum_{t=1}^{n}\left(C_t - \widehat{C}_t\right)^2}, \tag{13}$$

$$\mathrm{RE} = \frac{|\mathrm{RUL}^{\mathrm{pred}} - \mathrm{RUL}^{\mathrm{ture}}|}{\mathrm{RUL}^{\mathrm{ture}}}, \tag{14}$$

where the initial battery capacity value is indicated by C_t, the expected value is denoted by $\widehat{C}_t$. The expected remaining useful life is represented by $\mathrm{RUL}^{\mathrm{pred}}$, while the true remaining useful life is represented by $\mathrm{RUL}^{\mathrm{true}}$. The accuracy of RUL prediction increases when the MAE, RMSE, and RE approach zero. The outcomes are displayed in Algorithm 1.

Four network models, namely, the CEEMDAN-TCN, EMD-TCN, TCN, and LSTM, were employed in this study to predict the RUL of the NASA and CALCE datasets. Table 3 presents the prediction evaluation metrics for each model on the NASA dataset; in the case of B0006 battery, the MAE is reduced to 0.0689, the RMSE is reduced to 0.0828, and the RE is reduced to 0.0526. Table 4 shows the evaluation metrics for each model on the CALCE dataset.

Figures 12, 13 and 14 show how the LSTM, EMD-TCN and our approach fit the NASA and CALCE datasets. The results demonstrate that our method has a significantly better fitting influence than LSTM and EMD-TCN.

Comparing the prediction performance of the LSTM, TCN and EMD-TCN models on the NASA and CALCE datasets in Tables 3 and 4, we observe that the TCN model has a slight advantage over the LSTM in terms of accuracy. This demonstrates the superiority of the TCN in processing time-series battery data.

In terms of combining methods, the prediction error of the neural network model after CEEMDAN decomposition is lower than that of the single neural network model. The MAE, RMSE and RE error indicators are also superior to those of the single neural network model. To make the results more discernible, the basic parameters of the model used were configured as follows: number of iterations: 1000, size of the kernel: 3×1, Input_channel: 1, Output_channel: 10, Optimizer: Adam.

Algorithm 1. Proposed RUL prediction model.

Require: Extract battery capacity decay data, x; divide these datasets into training and testing sets.

Ensure: RUL prediction curves and evaluation index results.

1: Input battery capacity attenuation data set x.
2: Use $\overline{\mathrm{IMF}}_1 = \frac{1}{I}\sum_{i=1}^{I}\mathrm{IMF}_1^i$ to get n modal components IMF_i by CEEMDAN decomposition.
3: Use IMF_i to reconstruct datasets after data expansion.
4: Obtain output of the final battery capacity prediction data y processed by the TCN activation.
5: Calculate the RMSE, MAE, RE.
6: **return** RUL.

The performance of RUL prediction for all combined techniques on B0006 and CS2_35 is shown in Fig. 15. The experimental results show how well the CEEMDAN-TCN proposed in this study predicts the RUL of batteries and how highly accurate the prediction results are in comparison with a single model. The evaluation indicators demonstrate that our suggested model can make predictions that are more accurate. The NASA datasets show that the MAE and RMSE for the RUL of lithium-ion batteries are both below 0.0689 and 0.0828. The MAE and RMSE in the CALCE datasets are both below 0.0559 and 0.0736, respectively. The results show that our method's predictive performance is significantly greater and has stronger robustness when compared with a single neural network, suggesting that both feature extension and modal decomposition can improve model generalization.

5. Conclusions

In recent years, there has been growing interest in the prediction and health management (PHM) of lithium-ion batteries, where remaining useful life prediction is a critical means to ensure system security. Providing accurate RUL predictions is crucial for maintaining system reliability and safety.

Due to capacity regeneration and other objective factors, the original battery data are frequently noisy. In addition, the precipitation of lithium metal on the surface of the negative electrode results in a nonlinear decline in the lithium-ion battery capacity, which has an impact on the battery capacity reduction's ability to learn. The data can be expanded and the noise of the battery data can be reduced using CEEMDAN decomposition, which also helps the model perform better. The data can be increased to four times its original amount.

The TCN has a flexible receptive field that can be adjusted based on the number of layers, the size of the convolutional kernel, and the expansion coefficient

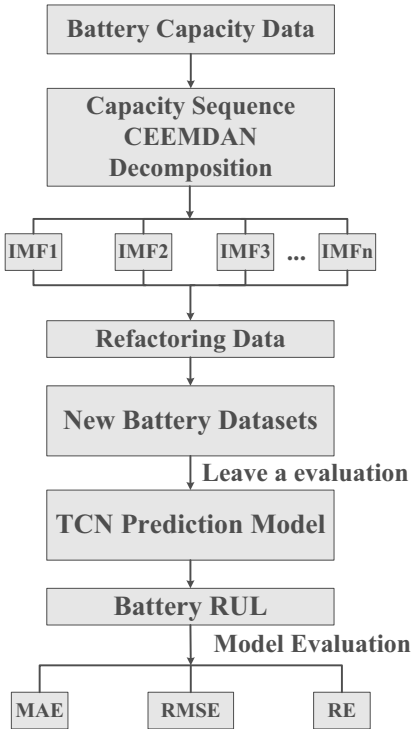

Fig. 11. Technology roadmap.

to accommodate various task-specific characteristics. Although recurrent neural network architectures are still commonly used in deep learning for sequence modeling, empirical evidence has demonstrated that the TCN can surpass these models in many tasks in terms of the predicted performance and efficiency.

A CEEMDAN-TCN framework for predicting the remaining useful life of lithium-ion batteries based on empirical modal decomposition and machine learning algorithms was proposed. Battery capacity was selected as the health indicator, and each fluctuation component of the battery capacity sequence data was decomposed using the CEEMDAN method to calculate their interpretation degree to the original data for integration and reconstruction. Feature dimensions are added to the time dimension of the original data to realize data expansion. The TCN model is then employed to predict the remaining service life of lithium-ion batteries. The validity of the proposed model is verified using the NASA and CALCE dataset collections, and the results show that the CEEMDAN-TCN framework is effective in predicting the RUL of lithium-ion batteries.

However, although our proposed network model is successful in the experiments of the existing NASA and CALCE datasets, there are still more possibilities to explore. We look forward to using more lithium battery data in a real environment to verify this method, which also requires more resources and hardware support. In the

Table 3. NASA prediction and evaluation index results.

Battery number	Neural network model	MAE	RMSE	RE
B0005	LSTM	0.0750	0.0876	0.2609
	TCN	0.0570	0.0695	0.2065
	EMD-TCN	0.0547	0.0685	0.1236
	Our approach	**0.0513**	**0.0617**	**0.0326**
B0006	LSTM	0.2623	0.2812	1.0000
	TCN	0.1129	0.1332	0.1437
	EMD-TCN	0.1037	0.1289	0.1711
	Our approach	**0.0689**	**0.0828**	**0.0526**
B0007	LSTM	0.1314	0.1391	0.5474
	TCN	0.955	0.1089	0.4808
	EMD-TCN	0.0711	0.0908	0.3942
	Our approach	**0.0506**	**0.0654**	**0.2044**
B0018	LSTM	0.0305	0.0362	0.0620
	TCN	0.0740	0.0892	0.2188
	EMD-TCN	0.0549	0.0681	0.0938
	Our approach	**0.0478**	**0.0612**	**0.0156**

Table 4. CALCE prediction and evaluation index results.

Battery number	Neural network model	MAE	RMSE	RE
CS2_35	LSTM	0.0746	0.1010	0.1638
	TCN	0.0713	0.0904	0.1207
	EMD-TCN	0.0467	0.0603	**0.0039**
	Our approach	**0.0393**	**0.0499**	0.1090
CS2_36	LSTM	0.1327	0.1684	0.1744
	TCN	0.0962	0.1267	0.1703
	EMD-TCN	0.0882	0.1113	0.1670
	Our approach	**0.0536**	**0.0736**	**0.1331**
CS2_37	LSTM	0.0293	0.0347	0.0169
	TCN	0.0694	0.0844	0.1816
	EMD-TCN	0.0311	0.0392	**0.0529**
	Our approach	**0.0270**	**0.0352**	0.0894
CS2_38	LSTM	0.0721	0.0797	0.1061
	TCN	0.0685	0.0651	0.0738
	EMD-TCN	0.0700	0.0906	0.1563
	Our approach	**0.0559**	**0.0538**	**0.0673**

future research, we will also consider further prediction of the number of battery life cycles and the state of charge of the battery to improve the prediction accuracy and performance of the overall algorithm model under different conditions.

Acknowledgment

This research has been financially supported by the following projects: *End Recovery Method and Mechanical Properties of Unmanned Autonomous Underwater Vehicles* (2022-Z05) and *Application Technology of Porous Medium Materials in Autonomous Underwater Vehicles* (2021-MS-034).

References

Bai, S., Kolter, J.Z. and Koltun, V. (2018). An empirical evaluation of generic convolutional and recurrent networks for sequence modeling, *arXiv* 1803.01271.

Cao, J., Li, Z. and Li, J. (2019). Financial time series forecasting model based on CEEMDAN and LSTM, *Physica A: Statistical Mechanics and Its Applications* **519**: 127–139.

Cao, Y., Ding, Y., Jia, M. and Tian, R. (2021). A novel temporal convolutional network with residual self-attention mechanism for remaining useful life prediction of rolling bearings, *Reliability Engineering & System Safety* **215**: 107813.

Chen, D., Hong, W. and Zhou, X. (2022). Transformer network for remaining useful life prediction of lithium-ion batteries,

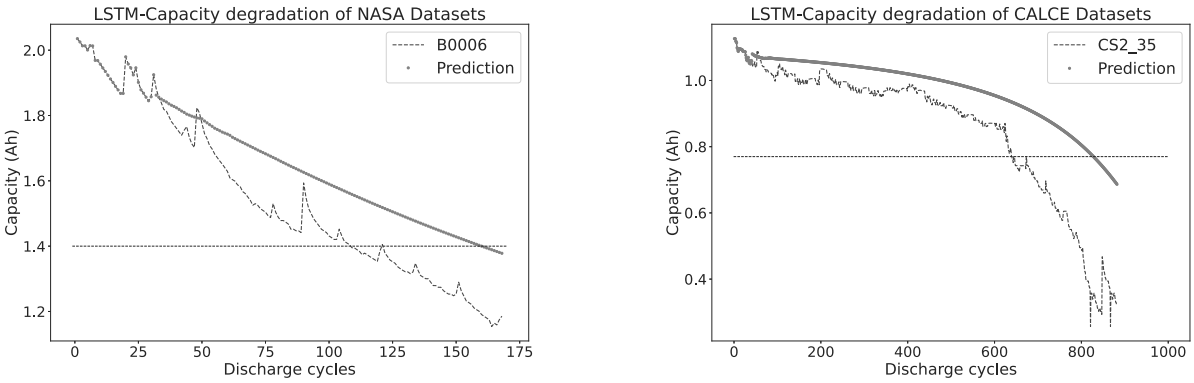

(a) (b)

Fig. 12. RUL prediction fitting effect of the LSTM network: NASA dataset (a), CALCE dataset (b).

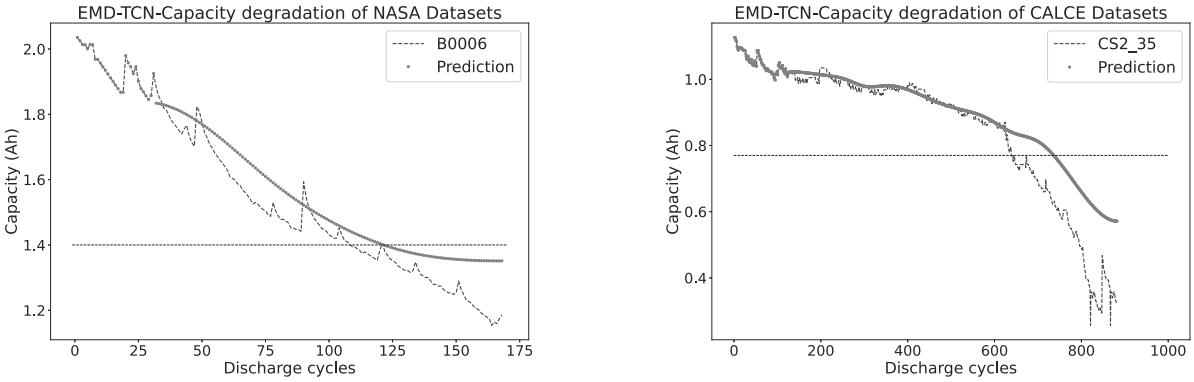

(a) (b)

Fig. 13. RUL prediction fitting effect of the EMD-TCN network: NASA dataset (a), CALCE dataset (b).

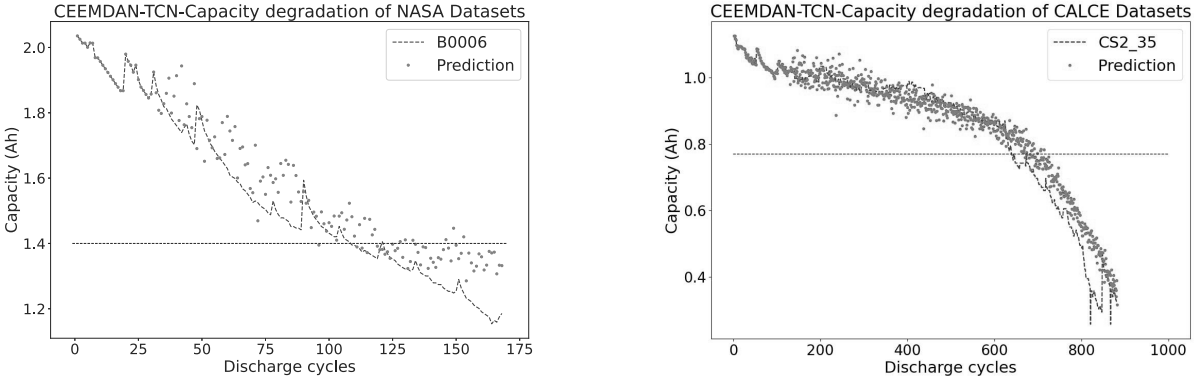

(a) (b)

Fig. 14. RUL prediction fitting effect of the CEEMDAN-TCN network: NASA dataset (a), CALCE dataset (b).

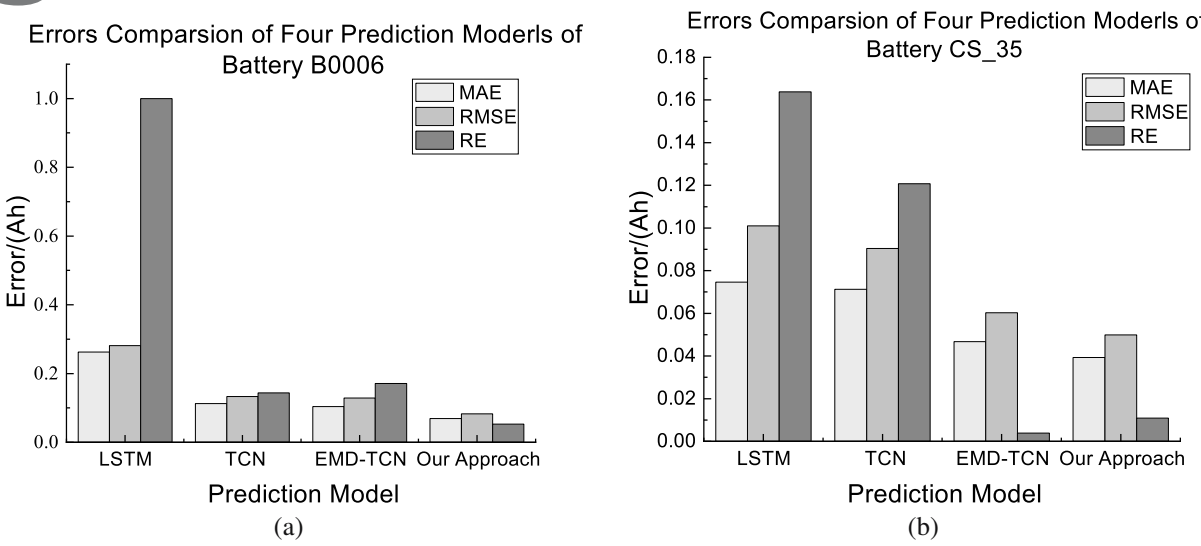

Fig. 15. Comparison of evaluation indicators for all combination methods: NASA dataset (a), CALCE dataset (b).

IEEE Access **10**: 19621–19628.

He, K., Zhang, X., Ren, S. and Sun, J. (2016). Deep residual learning for image recognition, *Proceedings of the IEEE Conference on Computer Vision and Pattern Recognition, Las Vegas, USA*, pp. 770–778.

Hong, S., Yue, T. and Liu, H. (2022). Vehicle energy system active defense: A health assessment of lithium-ion batteries, *International Journal of Intelligent Systems* **37**(12): 10081–10099.

Huang, N.E., Shen, Z., Long, S.R., Wu, M.C., Shih, H.H., Zheng, Q., Yen, N.-C., Tung, C.C. and Liu, H.H. (1998). The empirical mode decomposition and the Hilbert spectrum for nonlinear and non-stationary time series analysis, *Proceedings of the Royal Society of London A: Mathematical, Physical and Engineering Sciences* **454**(1971): 903–995.

Li, L., Li, Y., Mao, R., Li, L., Hua, W. and Zhang, J. (2023). Remaining useful life prediction for lithium-ion batteries with a hybrid model based on TCN-GRU-DNN and dual attention mechanism, *IEEE Transactions on Transportation Electrification* **9**(3): 4726–4740.

Li, X., Zhang, L., Wang, Z. and Dong, P. (2019). Remaining useful life prediction for lithium-ion batteries based on a hybrid model combining the long short-term memory and Elman neural networks, *Journal of Energy Storage* **21**: 510–518.

Park, K., Choi, Y., Choi, W.J., Ryu, H.-Y. and Kim, H. (2020). LSTM-based battery remaining useful life prediction with multi-channel charging profiles, *IEEE Access* **8**: 20786–20798.

Pecht, M. (2017). Battery data set: CALCE, *Battery Research Data*, CALCE Battery Research Group, University of Maryland, College Park, `https://calce.umd.edu/data#CS2`.

Ren, L., Zhao, L., Hong, S., Zhao, S., Wang, H. and Zhang, L. (2018). Remaining useful life prediction for lithium-ion battery: A deep learning approach, *IEEE Access* **6**: 50587–50598.

Saha, B. and Goebel, K. (2007). Battery data set: NASA, *NASA Ames Prognostics Data Repository*, NASA Ames Research Center, Moffett Field, `https://www.nasa.gov/intelligent-systems-division/#battery`.

Salimans, T. and Kingma, D.P. (2016). Weight normalization: A simple reparameterization to accelerate training of deep neural networks, *Advances in Neural Information Processing Systems* **29**(9): 901–909.

Seybold, L., Witczak, M., Majdzik, P. and Stetter, R. (2015). Towards robust predictive fault-tolerant control for a battery assembly system, *International Journal of Applied Mathematics and Computer Science* **25**(4): 849–862, DOI: 10.1515/amcs-2015-0061.

Srivastava, N., Hinton, G., Krizhevsky, A., Sutskever, I. and Salakhutdinov, R. (2014). Dropout: A simple way to prevent neural networks from overfitting, *Journal of Machine Learning Research* **15**(1): 1929–1958.

Torres, M.E., Colominas, M.A., Schlotthauer, G. and Flandrin, P. (2011). A complete ensemble empirical mode decomposition with adaptive noise, *2011 IEEE International Conference on Acoustics, Speech and Signal Processing (ICASSP), Prague, Czech Republic*, pp. 4144–4147.

Wu, Z. and Huang, N.E. (2009). Ensemble empirical mode decomposition: A noise-assisted data analysis method, *Advances in Adaptive Data Analysis* **1**(01): 1–41.

Ye, R. and Dai, Q. (2018). A novel transfer learning framework for time series forecasting, *Knowledge-Based Systems* **156**: 74–99.

Zhang, Y., Xiong, R., He, H. and Pecht, M.G. (2018). Long short-term memory recurrent neural network for remaining useful life prediction of lithium-ion batteries, *IEEE Transactions on Vehicular Technology* **67**(7): 5695–5705.

Zhou, B., Cheng, C., Ma, G. and Zhang, Y. (2020). Remaining useful life prediction of lithium-ion battery based on attention mechanism with positional encoding, *IOP Conference Series: Materials Science and Engineering*, **895**: 012006.

Zhou, Y. and Huang, M. (2016). Lithium-ion batteries remaining useful life prediction based on a mixture of empirical mode decomposition and ARIMA model, *Microelectronics Reliability* **65**: 265–273.

Jing Zhao received her BEng degree in mechanical automation in 2021. She is currently pursuing an MS degree at the Shenyang Institute of Automation, Chinese Academy of Sciences. Her research interests include prognostic health management (PHM) and deep learning.

Dayong Liu received his MS degree from the Shenyang Institute of Automation, Chinese Academy of Sciences, in 2007. He is currently a researcher at the same institute. He is mainly engaged in energy and power research of marine robots, including large-scale group management technology of marine robot lithium battery packs, safety control technology and independent management as well as distribution technology of hybrid electric power supply.

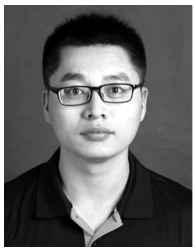

Lingshuai Meng received his PhD from the Shenyang Institute of Automation, Chinese Academy of Sciences, in 2020. He has been with Florida Atlantic University (USA) as a visiting scholar and is now an associate researcher at the Shenyang Institute of Automation. He is mainly engaged in marine robots, distribution and recycling related work.

Received: 15 March 2023
Revised: 31 August 2023
Re-revised: 28 October 2023
Accepted: 13 November 2023